Soares Diana (Orcid ID: 0000-0002-1485-6104)
Lisboa-Filho Paulo (Orcid ID: 0000-0002-7734-4069)
Bottino Marco (Orcid ID: 0000-0001-8740-2464)

Characterization of novel calcium-hydroxide mediated highly porous chitosan-calcium scaffolds for potential application in dentin tissue engineering

Diana Gabriela Soares
DDS, Ms, PhD, Assistant Professor, Department of Operative Dentistry, Endodontics and Dental Materials, Sao Paulo University – USP, Bauru School of Dentistry, Bauru, SP, Brazil. Al. Dr. Octavio Pinheiro Brizola, 9-75, Bauru, SP, Brazil. Postal code: 17012-901.
Ester Alves Ferreira Bordini
DDS, MS, PhD student, Department of Physiology and Pathology, Univ. Estadual Paulista – UNESP, Araraquara School of Dentistry, Araraquara, SP, Brazil. Humaita Street, 1680, Araraquara, SP, Brazil. Postal code: 14801-903.
Fernanda Balestrero Cassiano
Undergraduate student, Department of Physiology and Pathology, Univ. Estadual Paulista – UNESP, Araraquara School of Dentistry, Araraquara, SP, Brazil. Humaita Street, 1680, Araraquara, SP, Brazil. Postal code: 14801-903.
Erika Soares Bronze-Uhle
DDS, PhD, Department of Operative Dentistry, Endodontics and Dental Materials, Sao Paulo University – USP, Bauru School of Dentistry, Bauru, SP, Brazil. Al. Dr. Octavio Pinheiro Brizola, 9-75, Bauru, SP, Brazil. Postal code: 17012-901.
Leandro Edgar Pacheco
DDS, MS student, Department of Operative Dentistry, Endodontics and Dental Materials, Sao Paulo University – USP, Bauru School of Dentistry, Bauru, SP, Brazil. Al. Dr. Octavio Pinheiro Brizola, 9-75, Bauru, SP, Brazil. Postal code: 17012-901.
Giovana Zabeo
DDS, Ms, PhD student, Department of Operative Dentistry, Endodontics and Dental Materials, Sao Paulo University – USP, Bauru School of Dentistry, Bauru, SP, Brazil. Al. Dr. Octavio Pinheiro Brizola, 9-75, Bauru, SP, Brazil. Postal code: 17012-901.
Josimeri Hebling
DDS, MS, PhD, Professor, Department of Orthodontics and Pediatric Dentistry, Univ. Estadual Paulista – UNESP, Araraquara School of Dentistry, Araraquara, SP, Brazil. Humaitá Street, 1680, Araraquara, SP, Brazil. Postal code: 14801-903.
Paulo Noronha Lisboa-Filho
Ms, PhD, Professor, Department of Physics, Univ. Estadual Paulista – UNESP, School of Sciences, Bauru, SP, Brazil. Av. Eng. Luís Edmundo Carrijo Coube, 14-01, Bauru - SP, Brazil. Postal Code: 17033-360.
Marco Cicero Bottino
DDS, MSc, PhD, Associate Professor, Department of Cariology, Restorative Sciences, Endodontics, University of Michigan, School of Dentistry, Ann Arbor, MI, USA.
Carlos Alberto de Souza Costa

This is the author manuscript accepted for publication and has undergone full peer review but has not been through the copyediting, typesetting, pagination and proofreading process, which may lead to differences between this version and the Version of Record. Please cite this article as doi: 10.1002/jbm.b.34586

DDS, MS, PhD, Professor, Department of Physiology and Pathology, Univ. Estadual Paulista – UNESP, Araraquara School of Dentistry, Araraquara, SP, Brazil. Humaitá Street, 1680, Araraquara, SP, Brazil. Postal code: 14801-903.

Corresponding Author:
Prof. Dr. Diana Gabriela Soares
Department of Operative Dentistry, Endodontics and Dental Materials
Sao Paulo University – USP, Bauru School of Dentistry - FOB
Al. Dr. Octavio Pinheiro Brizola, 9-75, Bauru, SP, Brazil. Zip code: 17012-901.
+55-14-32358484
e-mail: soares.dg@usp.br

Abstract
The aim of this study was to develop a highly porous calcium-containing chitosan scaffold suitable for dentin regeneration. A calcium hydroxide ($Ca[OH]_2$) suspension was used to modulate the degree of porosity and chemical composition of chitosan scaffolds. The chitosan solution concentration and freezing protocol were adjusted to optimize the porous architecture using the phase-separation technique. Scanning electron microscopy/energy-dispersive spectroscopy demonstrated the fabrication of a highly porous calcium-linked chitosan scaffold (CH-Ca), with a well-organized and interconnected porous network. Scaffolds were cross-linked on glutaraldehyde (GA) vapor. Following a 28-day incubation in water, cross-linked CH scaffold had no changes on humid mass, and CH-Ca featured a controlled degradability profile, since significant humid mass loss was observed only after 21 (26.0%) and 28 days (42.2%). Fourier transform infrared spectroscopy (FTIR) indicated the establishment of Schiff base on cross-liked scaffolds, along with calcium complexation for CH-Ca. Cross-linked CH-Ca scaffold featured a sustained Ca^{2+} release up to 21 days in a humid environment. This porous and stable architecture allowed for human dental pulp cells (HDPCs) to spread throughout the scaffold, with cells exhibiting a widely stretched cytoplasm; whereas, the cells seeded onto CH scaffold were organized in clusters. HDPCs seeded onto CH-Ca featured significantly higher ALP activity, and gene expressions for ALP, Col1, DMP-1 and DSPP in comparison to CH, leading to a significant 3.5 times increase on calcium-rich matrix deposition. In sum, our findings suggest that CH-Ca scaffolds are attractive candidates for creating a highly porous and bioactive substrate for dentin tissue engineering.
KEYWORDS: Porous scaffolds, Chitosan, Calcium Hydroxide, Dental Pulp, Dentin.

1 INTRODUCTION

Tissue engineering approaches to repair and regenerate damaged tissues rely on the use of three-dimensional scaffolds that provide an extracellular matrix (ECM) template for cell infiltration and a physical support to guide the cells' activity into the targeted tissues or organs (Lei et al., 2018). These concepts have opened a new perspective for conservative treatments in Operative Dentistry and Endodontics, since, upon adequate stimulus, mesenchymal stem cells from pulp tissue and apical papillae are induced into

odontogenic phenotype and mediate the dentin-like tissue regeneration (Murray, 2012; Bottino et al., 2018). In the clinical scenario, calcium-hydroxide [$Ca(OH)_2$] powder, paste or cement, has been used as a mineralizing-inducer for dentin regeneration at pulp exposure sites. However, besides creating mineralized tissue on the application site, the burst release of Ca^{2+} and its high alkalinity instantly kills those cells in direct contact with the material, inducing an adjacent inflammatory reaction. Once the intensity of the inflammation is minimized and the Ca^{2+} gradient is established, dentin regeneration occurs, mediated by resident dental pulp cells (Sangwan et al., 2013; de Souza Costa et al., 2014; da Rosa et al., 2018). Therefore, tissue engineering strategies have focused on overcoming this negative initial effect by incorporating $Ca(OH)_2$ particles in polymeric blends to create smart biomaterials capable of modulating mineralized tissue regeneration. This is due to the complexation potential of Ca^{2+}, which modulates its release and, consequently, the local tissue pH, thus reducing inflammation intensity and improving tissue regeneration (Florez-Arriaga et al., 2018).

Chitosan scaffolds have been proven to provide adequate support for tertiary dentinogenesis in vivo (Yang et al., 2012; Li et al., 2014). A number of studies has shown that dental pulp cells seeded onto chitosan scaffolds remain viable and differentiate into odontoblast-like cells capable of depositing high amounts of calcium-rich matrix (Yang et al., 2012; Park et al., 2013; Soares et al., 2017; Soares et al., 2018). When chitosan is dissolved in acidic solutions, protonated free amino and hydroxyl groups are exposed, which allow chitosan to form ionic complexes with a wide variety of species, providing a simple mechanism for modifying the surface and bulk properties of the chitosan structures (Lei et al., 2017; Florez-Arriaga et al., 2018). Bonding -NH_2- and the -OH groups of chitosan with Ca^{2+} from mineral sources, can be obtained by simply mixing the mineral phase with the chitosan solution, enhancing interaction with precursor cells due to their increased similarity to natural bone/dentin ECM (Kim et al., 2015; Lei et al., 2017; Nitta et al., 2017; Soares et al., 2017; Klein-Júnior et al., 2018; Shahbazarab et al., 2018).

A highly interconnected porous network is also essential for host cell ingrowth, angiogenesis, and homogeneous neo-tissue-genesis throughout the scaffold structure (Gupte et al., 2018). Tri-dimensional porous chitosan scaffolds are usually obtained by freezing and lyophilizing chitosan solutions in a suitable vessel; however, these pores are fairly uniform, with a low degree of interconnectivity (Madihally & Matthew, 1999; Zhu et al., 2014; Aranaz et al., 2017). Porogens with a designed size and shape can be used to modulate pore architecture and interconnectivity, such as paraffin, sugar, salt, and silica; however, they require additional steps for porogen release (Ruixin et al., 2016; Ruixin et al., 2017; Wang et al., 2017). The gas foaming technique, by which carbon dioxide (CO_2) is injected into a polymeric solution, has also been used to increase overall porosity and pore interconnectivity (Harris et al., 1998). Others have described reactions between carbonate salts and weak acids as possibly resulting in a bubbling reaction from CO_2 release during the freezing process, which can control

the porous architecture of scaffolds. Carbonate sources are capable of donating Ca^{2+} to chitosan and, in turn, creating a fairly inexpensive and efficient Ca^{2+} drug release (Kim et al., 2008; Chen et al., 2012; Thein-Han et al., 2012; Chen et al., 2014; Sergeeva et al., 2015). These mineral phases can potentially modulate the osteo/odontogenic differentiation of bone/dentin precursor cells, and the increased deposition of hydroxyapatite on chitosan scaffolds has been demonstrated after incubation in simulated body fluid (Holopainen et al., 2014; Wang et al., 2016; Diaz-Rodriguez et al., 2018; Saveleva et al., 2018; Mohan et al., 2018).

In view of this, in the present investigation, we have proposed the addition of $Ca(OH)_2$ during fabrication of the chitosan scaffolds as a carbonate source to modulate the degree of porosity and donate Ca^{2+} for complexation. We intended to create a bioactive chitosan scaffold with a highly interconnected porous network capable of releasing Ca^{2+} in a sustained fashion in order to amplify the odontogenic potential of human dental pulp cells. Therefore, this new biomaterial would become an interesting candidate for pulp capping procedures by upregulating the regenerative potential of resident pulp cells with no tissue toxicity, thus leading to deposition of a dentin barrier at the exposure site.

2 MATERIALS AND METHODS

2.1 Development of macro-porous calcium-containing chitosan scaffolds

2.2.1 Scaffold synthesis: One or 2% high molecular weight chitosan solutions (310,000-375,000 Da; 75-85% deacetylated, pH 3.5, Sigma-Aldrich) were prepared by dissolving the powder into a 2% acetic acid aqueous solution at room temperature for 24 hours. A 1% w/v calcium-hydroxide ($Ca(OH)_2$; pH 12.0, Sigma-Aldrich) suspension was then prepared in deionized water. This suspension (2 mL) was incorporated dropwise under magnetic stirring (1,000-1,500 rpm) into 4 mL of chitosan solution (1:2), followed by a 5-min stirring at room temperature, to obtain chitosan-calcium-hydroxide solutions (pH 6.8). Incorporation of the $Ca(OH)_2$ suspension at low volumes under vigorous magnetic stirring allowed the mineral particles to be incorporated into the chitosan solution with no precipitation of the mineral phase. The $Ca(OH)_2$ suspension at 1% was chosen, since higher concentrations did not allow for its complete incorporation into the chitosan solution, and resulted in an extremely dry scaffold (*data not shown*). To obtain the scaffolds, as-received (unmodified) chitosan and chitosan-calcium-hydroxide solutions were poured into Teflon molds, frozen at -80^{o}C for 24 h and freeze-dried overnight (Liotop L101, Liobras, São Carlos, São Paulo, Brazil) at -56^{o}C. The scaffolds' morphology and composition were evaluated by scanning electron

microscopy (SEM)/energy-dispersive spectroscopy (EDS) (JMS-6610V Scanning Microscope; JEOL, Tokyo, Japan) at an accelerating voltage of 12-15 kV on samples sputter-coated with gold.

2.2.2 Evaluation of dental pulp cells' behavior: To assess the cytocompatibility of these formulations, a primary culture of dental pulp cells (HDPCs) were seeded onto the synthesized scaffolds for cell viability (Soares et al., 2018). A mixed culture of pulp cells was chosen to better represent the clinical scenario. The HDPC was obtained (after local Ethics Committee approval) by enzymatic digestion in a collagenase type I solution (3 mg/mL, Sigma-Aldrich, St. Louis, MO, USA) of fresh human pulp tissue from third molars (from an 18-year-old donor), as described in detail by Soares et al. (2018). Cells at passages 3 to 6 were used in this study. The scaffolds (6-mm diameter × 1-mm thick) were disinfected by soaking in 70% ethanol, followed by vacuum incubation for 30 min to eliminate air bubbles. The scaffolds were then placed on 48-well plates, washed in phosphate-buffered saline (PBS; pH 7.4; GIBCO), and incubated overnight at 37°C in complete α-MEM. The medium was delicately aspirated from the scaffolds, and one drop (3 μL) of α-MEM containing 1×10^5 HDPCs was poured onto the materials so that the cells were seeded exclusively on scaffold structures. The HDPC/scaffold constructs were then cultured for 24 h and incubated with 4 μM ethyl homodimer-1 (Eth-1 – dead cells = red fluorescence) and 2 μM Calcein AM (CA – viable cells = green fluorescence) in serum-free α-MEM at room temperature for 45 min (Live/Dead® Viability/Cytotoxicity Kit; Invitrogen). The presence of viable and dead cells on the scaffold was observed by means of a Leica DM 5500B microscope (Nussloch GmbH, Nussloch, Germany).

2.1.3 Modulating porosity degree by freeze-drying: The 2% high molecular weight chitosan solution containing 1% $Ca(OH)_2$ suspension (2:1) was selected and described as chitosan-calcium (CH-Ca) scaffold. The degree of porosity was modulated by varying the freezing method as follows: [-80°C] freezing at -80°C overnight; [-80°C/-198°C] freezing at -80°C overnight, followed by a 30-min immersion in liquid nitrogen (N_2); [-20°C/-80°C/-198°C] freezing at -20°C for 4 h, followed by freezing at -80°C overnight and 30-min immersion in N_2; [-20°C/-80°C] freezing at -20°C for 4 h, followed by freezing at -80°C overnight; [-198°C] 30-min immersion in N_2. Following the freezing procedure, the solutions were freeze-dried overnight (Liotop L101, Liobras) at -56°C. Scaffold surface topography was evaluated by SEM (JMS-6610V Scanning Microscope; JEOL). The scaffold porosity (%) and pore diameter (μm) were calculated by ImageJ software (National Institutes of Health, Bethesda, Maryland, USA) on 6 SEM images per sample (20 units per image) at 100× magnification (*n*=4).

2.1.4 Modulating degradation profile: In order to increase stability of the CH and CH-Ca scaffolds obtained by the gradual freezing protocol at -20°C/-80°C/-198°C, the

materials were cross-linked into 25% glutaraldehyde (GA) vapor. To that end, chitosan (CH) and CH-Ca scaffolds were prepared as previously described using the gradual freezing procedure (-20°C/-80°C/-198°C). The scaffolds (6-mm diameter × 1-mm thick) were placed in a platform inside a desiccator containing 15 mL of 25% glutaraldehyde solution at the bottom. A vacuum was applied for 30 min, and the set was incubated for 6 h. Degradability of the CH and CH-Ca scaffolds subjected or not to cross-linking was assessed by calculating the humid weight over 28 days (n = 6). The samples were incubated in a 500 μL PBS solution at 37°C for 1 h, followed by drying with absorbent paper at 37°C for 30 min for initial humid weight measurement (baseline) in a micro-precision meter (Mettler Toledo XS105 DualRange). Immediately thereafter, the samples were incubated in PBS at 37°C for 4 weeks, with the PBS solution being replaced at every week. The weight was measured following 1 day of PBS incubation, and weekly from the baseline. A total for 3 readings were performed at each measurement. The mean baseline value for each material was considered to be 100% of the humid weight in order to calculate the percentage of humid mass throughout the degradation period.

2.1.5 Fourier-transform infrared spectroscopy (FTIR) analysis: The unmodified chitosan (CH) and CH-Ca scaffolds, subjected or not to cross-linking were assessed using FTIR to detect modifications on the chitosan spectra due to $Ca(OH)_2$ incorporation and GA vapor. This analysis was performed to understand the chemical interaction of $Ca(OH)_2$ with chitosan and predict its release potential in an humid environment. The spectra were recorded in a Shimadzu FT-IR-8300 (Shimadzu Corporation, Kyoto, Honshu, Japan) with an average accumulation of 32 scans between 4500 to 400 cm^{-1} with a resolution of 4 cm^{-1} at room temperature, in attenuated total reflectance (ATR) mode. The samples (n=3) were positioned in the center of an ATR diamond crystal (Smart Miracle™, Pike Technologies, Madison, WI, USA) and compressed against with a micrometric low-pressure clamp (Shimadzu Corporation).

2.1.6 Calcium release: This analysis was performed on cross-linked CH and CH-Ca scaffolds by immersing the cylindrical samples in 200 μL of ultra-pure distillated water (Life Technologies) at 37°C, for 1, 5, 7, 14, and 21 days (n=4). At each time-point, one aliquot was removed for reading by reaction with o-cresolphtalein complexone substrate (Labtest, Lagoa Santa, MG, Brazil). The absorbance was quantified at 570 nm (Synergy H1, Biotek, Winooski, VT, USA) and the data was converted in concentration (mg/dL) by means of a standard curve.

2.2 Biological characterization of cross-linked chitosan-calcium scaffolds

2.2.1 Cell viability, spreading, and proliferation: HDPCs were seeded onto cross-linked CH and CH-Ca samples and cell viability (n=2) was evaluated by live/dead assay, such as previously described, after culturing the cell/scaffold construct in complete α-MEM for 14 days. F-actin staining was performed at the material's surface and in 1-mm thick transversal slices to observe the cytoplasmic filaments morphology throughout the scaffolds after 14 days of in vitro culture. The constructs (n=2) were fixed in 4% paraformaldehyde for 15 min at room temperature, followed by washing in PBS and incubation with Alexa-fluor Phalloidin 555 in 2% bovine serum albumin (1:40 Life Technologies) for 30 minutes. The samples were washed in PBS, covered with mounting medium with DAPI (Life Technologies), and evaluated on a fluorescence microscope (Leica DM 5500B, Nussloch GmbH). Alamar Blue® assay (n=6) was performed at 1, 7, and 14 days of cell culture, for indirect measurement of cell proliferation over time. At each time point, the constructs were incubated with 1:10 Alamar Blue® dye in serum-free medium for 4 h at 37°C and 5% CO_2. The fluorescence intensity of the supernatant was read at 570 nm excitation and 585 nm emission (Synergy H1; Biotek). The mean absorbance values of the CH group at day 1 was considered to be 100% of cell viability to determine proliferation over time for both the CH and CH-Ca scaffolds.

2.2.2 ALP activity: This parameter was measured at 14 days of the HDPC/scaffold culture by means of the SensoLyte™ Alkaline Phosphatase Assay Kit (AnaSpec; Fremont, CA, USA). The scaffolds (n=6) were transferred to 1.5 mL tubes, immersed in Triton-X 100 for cell lysis, and subjected to mechanical disruption with a pestle tissue grinder. P-nitrophenyl phosphate colorimetric substrate was then added and the samples were incubated at room temperature for 1 h. The samples were then centrifuged at 10,000 *g* at 4°C for 15 min to collect the supernatant, and the absorbance was read at 405 nm (Synergy H1, Biotek). Data was obtained by means of a standard curve and normalized using the total protein content (Lowry/Folin-Ciocalteu method) (Soares et al., 2018). The CH-group was considered to be 100 % of the ALP activity.

2.2.3 Mineralized matrix deposition: The cell-scaffold constructs (n=6) at 21 days were fixed in 70% ethanol at 4°C for 1 h, followed by washing in PBS, and staining with 40 mM Alizarin Red (Sigma-Aldrich) solution for 20 min. The scaffolds were submitted to a 5-time washing in deionized water under shaking for 15 min. Thereafter, the samples were transferred to 1.5 mL tubes, immersed in 10% cetylpyridinium chloride, mechanically disrupted with a pestle, and incubated at room temperature for 20 min. The supernatant was collected (10,000 *g* at 4°C for 15 min), which was used for absorbance reading at 570 nm (Synergy H1, Biotek). Scaffolds with no cells were used as blanks for each composition, eliminating the background (these samples followed

the same experimental protocol as cell-seeded scaffolds). The CH group was considered to represent 100% of the mineralized matrix deposition.

2.2.4 Real-time PCR: Gene expression of DSPP, DMP-1, ALP, and collage type I (Col1) was evaluated by real-time PCR at 21 days (n = 4), by using an RNAqueous®-micro kit (Ambion, Austin, TX, USA) and a High Capacity cDNA Reverse Transcription Kit (Applied Biosystems, Foster City, CA, USA), according to the recommended protocol for RNA isolation and cDNA synthesis, respectively. Real-time PCR quantification of mRNA (StepOne Plus; Applied Biosystems) was performed with Taqman assays and reagents (Applied Biosystems). GAPDH was used as the constitutive gene. Data were calculated according to the $2^{\Delta\Delta CT}$ equation, with the CH group for normalization.

2.3 Statistical analysis

Two independent experiments were performed. Data were compiled and analyzed by one- or two-way ANOVA followed by the Tukey's test for observation of significant differences between the study groups or by the Student's test ($p < 0.05$ = statistically significant). Power calculation analysis was performed by DDS Research (Statistical Power Calculator, average, two-sample, two-tailed test, α=5%) at the end of the experiment, showing 100% statistical power for each evaluation.

3 RESULTS

3.1 Structure and chemical analysis of the scaffolds

Plain chitosan scaffolds prepared with a 1% or 2% chitosan solution featured a disorganized porous architecture, as observed in the SEM images on Fig. 1a/c. Nevertheless, when the mineral phase composed by 1% $Ca(OH)_2$ suspension was incorporated, the scaffolds featured a more organized pore network, with a round-shaped architecture. EDS analysis demonstrated the presence of Ca in the chitosan composition (Fig. 1b/d), and live/dead images confirmed the cytocompatibility of all tested formulations with HDPCs. Among the tested formulations, the 2% high molecular weight chitosan solution gave rise to larger pores, allowing for the HDPCs to exhibit a stretched cytoplasm 24 h after seeding; whereas, the cells were organized into clusters for all the other formulations. Therefore, this formulation was selected and described as chitosan-calcium scaffold (CH-Ca) for the following experiments. This formulation was then subjected to different freezing protocols to select the one capable of providing the larger pore diameter and higher degree of porosity. The SEM images in Fig. 2a demonstrated that all freezing protocols gave rise to round-shaped porous scaffolds with different architectures. Analysis of the pore diameter (Fig. 2b) demonstrated that freezing CH-Ca at -80°C, -20°C/-80°C, -20°C/-80°C /-198°C resulted in the highest pore size in comparison to the other protocols, with no significant differences among them. Nevertheless, analysis of the porosity degree showed that

gradual freezing at -20°C/-80°C/-198°C conferred a significantly higher percentage of porosity among all tested protocols (Fig. 2c). Therefore, this protocol was selected for the following experiments.

3.2 FTIR analysis of CH and CH-Ca scaffolds

Fig. 3a shows the FTIR spectra of the CH scaffold (pure chitosan) and CH-Ca scaffold. In pure CH scaffold, several characteristic absorbance bands were identified: 1) The broad band around 3500–3100 cm^{-1}, relative to the stretch vibrations of the -OH and –NH groups; 2) The band at 2929 and 2875 cm^{-1}, related to the asymmetric and symmetric C–H stretch vibration of the CH groups; 3) The vibrational bands of amide I, amide II, and amide III, situated at 1650, 1552, and 1321cm^{-1}, respectively; 4) The asymmetric -NH_2 bending vibration situated at ∼1590-1560 cm^{-1} overlaps with the amide II band. Thus, characteristic -NH bend vibrations in primary amines are situated at 1639 cm^{-1} (CO-NHR) and are relative to the protonated amino group. In general, this band, relative to amines on –CO-NHR and –C=O of amide, appears in the same regions of frequency (1600-1650 cm^{-1}) in the FTIR spectrum; 5) The NH_2 bend vibrations coupled with the -C-N stretching of amide II, are observed at 1552 cm^{-1}; and the -C-N stretching band of amide, coupled with the -NH bend, appears around 1321-1380 cm^{-1}; 6) Bands at 1408, 1380 and 1257 cm^{-1} region are also related to -CH symmetrical deformations bend of alkyl and the methyl groups; 7) The absorption bands at 1153, 1074, and 1029cm^{-1} are indicative of the C-O stretching vibrations [(C-O-C)] bridge and skeletal vibrations] of the polysaccharide structure; 8) The absorption band at 896 cm^{-1} is also characteristic of the saccharide structure of chitosan. The CH-Ca spectra featured a marked displacement in the position and change of intensity, denoting the interaction of chitosan with $Ca(OH)_2$. The absorption bands at (1608, 1567, 1534, 1469 and 1447 cm^{-1}) showed an increased modification after the insertion of $Ca(OH)_2$. Bands at 1608, 1567, and 1534 cm^{-1} relatives to -NH stretching and bending vibrations of amides and amines (-NH_2, -NHCO, and -C-N) presented a marked intensity and shift change, indicating involvement of the amino groups in the calcium complex formation. New bands at 1469 and 1442 cm^{-1} are relative to suggest a different arrangement of primary hydroxyl groups and modification in the CH_2-OH environment and carbonated stretching of CO_3^{2-}. A decrease of the band at 1153 and 1072 cm^{-1} for -C-O stretching vibrations indicates the complexation of Ca^{2+} with the hydroxyl and acetyl groups of the saccharide structure. The appearance of bands in the low frequency region (670-644 cm^{-1}) is referent to stretching vibrations of the Ca-N and Ca-O bonds.

Fig. 3b-d shows FTIR spectra derivates after cross-linking. It is possible to observe that amide I and amide II band on cross-linked CH scaffold shows shift and intensity alterations, with absorbencies in the range of 1645-1348 cm^{-1} , relative to reticulation reaction between chitosan amine –NH_2 groups and C = O groups of GA, to form imines -C = N (Fig. 3b). It is noteworthy, that bands related to the imine-type bonds (-C = N) may overlap the C=O-type bands of amide I, since both absorb in the same region of the infrared spectrum. Another significant change occurred in the region of 1565-1530

cm^{-1} strongly indicating C = C bonds. Changes on CH-Ca spectra can also be noted after cross-linking (Fig. 3c) at -NH stretching and bending vibrations of amides and amines (-NH_2, -NHCO and -C-N, at 1567, 1534 and 1447 and 1415 cm^{-1}) indicating GA interaction in these binding sites. Additionally, a decrease of the band at 1608 cm^{-1} and the appearance of the band at 1644 cm^{-1} relative to imine, also indicates effective GA cross-linking, and the new bands in the region of 1380 and 1310 cm^{-1} demonstrates the establishment of Shiff base. Finally, when CH and CH-Ca spectra after the interaction with GA were compared (Fig. 3d), it is possible to notice the spectral differences related to the interaction and presence of calcium in the scaffold structure, indicating that even after GA cross-linking, Ca complexation was stablished.

3.3 Analysis of degradability degree

As demonstrated in Table 1, both CH and CH-Ca had high degradation rate when immersed in a neutral aqueous medium without GA cross-linking. Significant weight loss in comparison to the baseline occurred at 7, 14, 21, and 28 days for the CH scaffold, with each being around 32.0%, 74.3%, 83.9%, and 85.9%, respectively. CH-Ca featured a significantly higher degradability than CH at day 1, losing around 28.9% mass in comparison to the baseline, followed by 54.9%, 84.3%, 91.4%, and 94.2% of weight loss at, 7, 14, 21, and 28 days, respectively. These degradability profiles were significantly reduced for both scaffolds when they were subjected to GA-crosslinking. For CH, no significant differences were observed for humid mass throughout the time-points, and significantly higher values were detected in comparison to non-crosslinked CH scaffolds at day 7, 14, 21, and 28. A similar pattern was detected for CH-Ca. No significant difference from the baseline was observed for the GA-treated CH-Ca scaffolds on days 1, 7, and 14. Significant mass loss of around 26.0% and 42.2%, respectively, in comparison to the baseline was observed at 21 and 28 days, respectively. Significant differences between GA-treated scaffolds was detected only at 28 days, demonstrating that GA-treated CH-Ca scaffold had a significantly higher degradability degree than GA-treated CH scaffold following a long incubation time in a humid environment.

3.4. Degree of architecture and porosity for GA-treated scaffolds

SEM images of a GA-treated scaffold's surface and transversal slices (Fig. 4a/d) demonstrate that the cross-linked CH-Ca scaffold featured an organized and interconnected porous network; whereas, the CH scaffold had a disorganized, porous architecture. This macro-porous architecture was detected on the surface and in transversal slices of the CH-Ca, thus demonstrating the potential for this formulation to create a homogeneous matrix for tissue engineering. A significantly higher pore diameter was detected for the CH-Ca scaffold (202.1 μm) in comparison to the CH scaffold (86.9 μm). The percentage of porosity was also significantly higher for CH-Ca (86.89%) related to CH (32.17%) (Fig. 4e/f).

3.5. Analysis of calcium release.

The cumulative calcium (Ca^{2+}) release profile from the CH and CH-Ca scaffolds is demonstrated in Fig. 5. A sustained Ca^{2+} release was detected for the CH-Ca scaffold throughout the time-points, with the higher amount being detected at 21 days, demonstrating that a Ca^{2+} release system was achieved.

3.6. In vitro biological characterization.

According to Fig. 6a, significantly higher cell viability values were detected for CH-Ca as compared to CH at 1 and 7 days, demonstrating a higher proliferative potential for the cells seeded onto the CH-Ca scaffold. The live/dead images at 14 days confirm the presence of viable cells at the surface of both scaffolds (Fig. 6b). F-actin images revealed that cells were capable of spreading throughout the porous structure of CH-Ca; whereas, round-shape structures were detected on the CH scaffold (Fig. 6c/d). Significant increases in ALP activity and mRNA gene expression of the odontoblastic markers ALP, Col1, DMP-1 and DSPP were observed for CH-Ca in comparison to the CH scaffold, along with a significant increase (3.5×) in mineralized matrix deposition detected by the alizarin red assay (Fig. 7a-f).

4 DISCUSSION

Chitosan solutions can be easily transformed into porous, spongy-like structures using the phase-separation technique. Ice induces the solute originally dispersed into the solution to be segregated; once eliminated by freeze-drying, ice creates polygonal pores at the material structure (Madihally, Matthew 1999; Zhu et al., 2014; Aranaz et al., 2017). Incorporation of a mineral phase to chitosan scaffolds has been proposed to enhance osteoconductivity and fasten neo-tissue-genesis. Usually, the material is prepared by mixing the powder in a chitosan solution; however, by using this protocol, mineral forms aggregates that interfere with the rheological behavior of the chitosan solution, as high viscosity suspensions prevent water migration for the growth of ice crystals, thus reducing pore size and interconnectivity (Kim et al., 2015; Lei et al., 2017; Nitta et al., 2017; Soares et al., 2017; Klein-Júnior et al., 2018; Shahbazarab et al., 2018). In the present investigation, we proposed to incorporate $Ca(OH)_2$ aqueous suspension into the chitosan solution to modulate both, the degree of porosity and chemical composition. According to our results, the incorporation of a 1% $Ca(OH)_2$ suspension into a 2% chitosan solution subjected to a gradual freezing protocol at -20°C/-80°C/-198°C, gave rise to a highly porous scaffold containing calcium within its structure, as demonstrated in the chitosan-calcium scaffold (CH-Ca).

The increased pore size and pore-interconnectivity detected on the CH-Ca scaffolds could be the result of a chemically-mediated bubbling effect. Previous studies have demonstrated utilization of the foam method to increase pore size and pore-interconnectivity by reacting calcium carbonate ($CaCO_3$) or calcium bicarbonate ($NaHCO_3$) and weak acids (citric acid) to generate CO_2 bubbles, giving rise to an

organized, macroporous architecture (Kim et al., 2008; Chen et al., 2012; Thein-Han et al., 2012; Chen et al., 2014). According to the literature, dissolution of $Ca(OH)_2$ in water results in the absorption of atmospheric CO_2 and the formation of carbonate ions (CO_3^{2-}), ultimately leading to the formation of a $CaCO_3$ layer on the surface of $Ca(OH)_2$ particles (Savija; Lukovic, 2016). The FTIR data of the CH-Ca scaffold suggests the occurrence of this phenomenon, since we observed the incorporation of a peak in the 1400-1500 cm^{-1} range, which corresponds to CO_3^{2-} precipitation band (Plavsic et al. 1999) supporting the mechanism of the bubbling formation. Therefore, we believe that $Ca(OH)_2$ water suspension reacted with air-bubbles entrapped in the chitosan solution due to vigorous stirring, which then acted as a source of CO_2, leading to the formation of a $CaCO_3$-rich phase on $Ca(OH)_2$ particles. Following this process, the reactions of $Ca(OH)_2$ and $CaCO_3$ with acetic acid from the chitosan solution may have allowed for the formation of calcium acetate ultimately releasing CO_2 after reacting with $CaCO_3$. Calcium acetate has been proven to sequestrate CO_2 (Kim; Kim, 2018; Vinoba et al., 2013), thus facilitating the bubbling effect due to expansion of the entrapped air inside the chitosan solution, increasing pore size. The molecular movement of the ions during these reactions may have created the pore interconnections observed for in CH-Ca scaffold. The increased degree of porosity could also be a result of the water content of the CH-Ca solution, reducing the viscosity of the solvent phase compared to the CH solution, thus allowing for the development of larger ice crystals (Kim et al., 2015). Gradual freezing may have allowed the ice crystals to grow in size (Madihally, Matthew 1999; Zhu et al., 2014), playing a role in the establishment of macropores after freeze-drying.

Sergeeva et al. (2015) described a mechanism of pore enlargement and interconnectivity on alginate scaffolds by using $CaCO_3$ as a porogen; however, this process also led to the release of Ca^{2+}, which was capable of binding to the alginate structure. Therefore, $CaCO_3$ acted as a CO_2 precursor and calcium donor. A similar effect was detected in the present investigation. Besides modulating the pore architecture of the chitosan scaffolds, $Ca(OH)_2$ also resulted in the assimilation of Ca on the chitosan structure, as determined by EDS analysis (Fig. 1). Chitosan is able to interact with various metal ions due to the presence of ionizable amine and hydroxyl functional groups on the chitosan surface. Whereas metal anions are bound to chitosan by electrostatic attraction, metal cation, such as Ca^{2+}, is likely to form ligands (Pestov; Bratskaya, 2016). The modifications on the FTIR spectra of CH-Ca scaffold, suggests deprotonation of the of the NH_3^+ groups due to treatment with $Ca(OH)_2$. The variations on intensity and shift change of the bands are relative to stretching and bending vibrations of amides and amines (-NH_2, -NHCO and -C-N), indicating the involvement of amino groups in the calcium complex formation. We may also suggest an interaction of Ca^{2+} with hydroxyl and the acetyl groups of the saccharide structure, due to the appearance of bands in a low frequency region (670-644 cm^{-1}), which refers to the stretching vibrations of Ca-N and Ca-O bonds (He et al., 2011). The amino, hydroxyl and acetyl groups present on the chitosan surface are the main sites of

interaction with metallic ions forming stable complexes by coordination, functioning as ligands (Pestov; Bratskaya, 2016). According to the literature, this bonding is favored at a higher pH, as deprotonated amine groups ($-NH_2$) that can bind to Ca^{2+}, thus minimizing electrostatic repulsion of the positively charged amide groups ($-NH_3^+$) found at a low pH (Florez-Arriaga et al., 2018). In our experiment, the pH of the Ca-free chitosan solution in 2% acetic acid was around 3.5, which was then increased to 6.8 after incorporation of a highly alkaline $Ca(OH)_2$ (pH 12.0) suspension (Vold et al., 2003).

Following the development of CH-Ca scaffolds, we detected a high sensitivity to water contact, as demonstrated by the degree of degradation. Therefore, the Ca-free chitosan (CH) and CH-Ca scaffolds were subjected to cross-linking with glutaraldehyde (GA) vapor for 6 h to control the degradation rate. Analysis of FTIR spectra demonstrated the creation of Schiff base in both scaffolds, and it did not interfere with Ca complexation on CH-Ca scaffold. GA treatment markedly reduced degradation for both scaffolds; it also allowed for pore architecture maintenance, as observed in the SEM images. Therefore, a stable artificial ECM to support neo-tissue-genesis with 86.89% of degree of porosity and 202.1 μm pore size was obtained. Previous reports demonstrated that incubation in GA vapor is capable of increasing the mechanical properties and reducing degradability of the delicate chitosan-containing nanofibers, maintaining the matrix architecture (Chen et al., 2010; Liu et al., 2017). According to Zhu et al. (2017), GA vapor incubation for long periods (24-48 h) causes modifications on scaffold nano- and micro-architecture and creates very stiff matrices with toxic potential. On the other hand, 2-6 h GA vapor treatment causes less than a 1% modification in the scaffold architecture, thus significantly increasing its mechanical properties and reducing its degradability due to the creation of Schiff base (C=N) through the GA aldehyde groups' reaction with primary amines. When mesenchymal stem cells were seeded onto 6 h GA vapor-treated scaffolds, the cells were capable of adhering and similarly spreading as seen in non-cross-linked matrices. Nevertheless, long-term treatments, such as 48 h, turn the substrate toxic, which does not allow the establishment of cell-matrix interactions (Zhu et al., 2017). In our experiment, the cells were seeded onto GA-treated scaffolds, with no toxic effect being detected. Of note, the interconnected porous network of CH-Ca allowed viable cells with stretched cytoplasm to spread throughout the scaffold structure. On the other hand, cells seeded on CH scaffolds were organized into clusters resembling the scaffold architecture. Cell proliferation was enhanced for the CH-Ca scaffolds at initial periods, which may have occurred due to increased superficial area and adequate scaffold composition (Kim et al., 2015).

The cross-linked CH-Ca scaffold promoted a sustained Ca^{2+} release over time, which is an important feature for biological functions. Farhadian et al. (2018) demonstrated that chitosan/gelatin can act as a nanocarrier system for $Ca(OH)_2$ delivery. The authors incorporated an aqueous solution of $Ca(OH)_2$ into a chitosan/gelatin solution under intense magnetic stirring for 5 min to obtain a homogeneous solution, followed by freeze-drying, similarly to what was performed in

the present investigation. Then, smooth surface particles with controlled-prolonged Ca^{2+} release were obtained. Florez-Arriaga et al. (2018) demonstrated that $Ca(OH)_2$ pastes containing chitosan as a vehicle successfully promoted a sustained release of Ca^{2+} over time. However, these authors did not evaluate the biological functions of these biomaterials. Klein-Júnior et al. (2018) created a biomembrane of bovine pericardium coated with a chitosan layer containing $Ca(OH)_2$ particles for direct pulp capping. This material was applied on the mechanically exposed pulp tissue of rats, and the authors observed that the pulp tissue in contact with the $Ca(OH)_2$-chitosan-biomembrane was less disorganized and inflamed, when compared to the $Ca(OH)_2$ paste. The authors reported that this positive result was related to the slow degree of Ca^{2+} release mediated by the experimental biomembrane. In the present study, the osteo/odontogenic markers expression denoted the bioactive potential of the CH-Ca scaffold. This biomaterial up-regulated gene expressions of ALP, Collagen type I, DSPP, and DMP-1, while it also increased ALP activity and the mineralized matrix deposition. These biological effects may be related to the Ca^{2+} influx into the intracellular environment with activation of unspecified Ca^{2+} channels, thus enhancing cell proliferation and activating ERK1/2 signaling along with DSPP, ALP, fibroblast growth factor 2 (FGF-2), OPN, and OCN overexpression (Rashid et al., 2003; An et al., 2012; Barradas et al., 2012; Wo et al., 2013; Li et al., 2015; Kanaya et al., 2018; Kulan et al., 2018). Activation of SMAD 1/5/8 signaling pathways and increasing BMP-2 expression has also been closely related to osteogenic differentiation of precursor cells in contact with calcium-releasing sources (Li et al., 2015; Kanaya et al., 2018).

Therefore, the innovative scaffold developed herein represents a new approach to creating a low-cost, highly porous artificial extracellular matrix capable of acting as a drug release system for Ca^{2+}, using a naturally-derived polymer. The in vitro analysis demonstrated the bioactive potential with human dental pulp cells toward an odontogenic phenotype; however, in vivo studies are necessary to observe the potential of CH-Ca as a promising biomaterial for dentin regeneration.

5 CONCLUSION

This study reports a simple approach to modulating the architecture and chemical composition of chitosan scaffolds by incorporating a $Ca(OH)_2$ suspension during the formulation procedure using the phase-separation technique. A highly porous and stable calcium-linked chitosan scaffold was created and its architecture controlled human dental pulp cell proliferation. The calcium incorporated into the chitosan structure was released, creating an environment capable of positively modulating human dental pulp cells odontogenic differentiation evidenced by the deposition of high amounts of calcium-rich matrix when compared to Ca-free chitosan scaffolds. In sum, the low-cost, innovative porous chitosan-calcium scaffold developed in this study seems to be a viable candidate for mineralized tissue (dentin) regeneration.

ACKNOWLEDGMENTS

This work was supported by the São Paulo Research Foundation – FAPESP (grants # 2013/23520-0 and 2016/15674-5), and by the Coordenação de Aperfeiçoamento de Pessoal de Nível Superior - CAPES – (Finance Code 001).

REFERENCES

1. Lei, B., Guo, B., Rambhia, K.J., Ma, P.X. (2018). Hybrid polymer biomaterials for bone tissue regeneration. *Frontiers in Medicine*, doi: 10.1007/s11684-018-0664-6. [Epub ahead of print].
2. Murray, P.E. (2012). Constructs and scaffolds employed to regenerate dental tissue. *Dental Clinics of North America, 56*(3), 577-88.
3. Bottino, M.C., Pankajakshan, D., Nör, J.E. (2017). Advanced Scaffolds for Dental Pulp and Periodontal Regeneration. *Dental Clinics of North America, 61*(4), 689-711
4. Sangwan, P., Sangwan, A., Duhan, J., Rohilla, A. (2013). Tertiary dentinogenesis with calcium hydroxide: a review of proposed mechanisms. *International* Endodontic Journal, 46(1), 3-19.
5. de Souza Costa, C.A., Hebling, J., Scheffel, D.L., Soares, D.G., Basso, F.G., Ribeiro, A.P. (2014). Methods to evaluate and strategies to improve the biocompatibility of dental materials and operative techniques. *Dental Materials, 30*(7), 769-84.
6. da Rosa, W.L.O., Cocco, A.R., Silva, T.M.D., Mesquita, L.C., Galarça, A.D., Silva, A.F.D., Piva, E. (2018). Current trends and future perspectives of dental pulp capping materials: A systematic review. *Journal* of *Biomedical* Materials *Research* Part *B*: Applied *Biomaterials*, *106*(3), 1358-1368.
7. Flores-Arriaga, J.C., Pozos-Guillén, A.J., González-Ortega, O., Escobar-García, D.M., Masuoka-Ito, D., Del Campo-Téllez, B.I.M., Cerda-Cristerna, B.I. (2018). Calcium sustained release, pH changes and cell viability induced by chitosan-based pastes for apexification. *Odontology,* doi: 10.1007/s10266-018-0389-7. [Epub ahead of print]
8. Yang, X., Han, G., Pang, X., Fan, M. (2012). Chitosan/collagen scaffold containing bone morphogenetic protein-7 DNA supports dental pulp stem cell differentiation in vitro and in vivo. *Journal of Biomedical Materials Research Part A,* doi: 10.1002/jbm.a.34064. [Epub ahead of print]
9. Li, F., Liu, X., Zhao, S., Wu, H., Xu, H.H. (2014). Porous chitosan bilayer membrane containing TGF-β1 loaded microspheres for pulp capping and reparative dentin formation in a dog model. *Dental Materials, 30*(2), 172-181.
10. Park, S.J., Li, Z., Hwang, I.N., Huh, K.M., Min, K.S. (2013). Glycol chitin-based thermoresponsive hydrogel scaffold supplemented with enamel matrixderivative promotes odontogenic differentiation of human dental pulp cells. *Journal of Endodontics, 39*(8), 1001-1007.
11. Soares, D.G., Rosseto, H.L., Scheffel, D.S., Basso, F.G., Huck, C., Hebling, J., de Souza Costa, C.A. (2017). Odontogenic differentiation potential of human dental pulp cells cultured on a calcium-aluminate enriched chitosan-collagen scaffold. *Clinical Oral Investigation, 21*(9), 2827-2839.

12. Soares, D.G., Anovazzi, G., Bordini, E.A.F., Zuta, U.O., Silva Leite, M.L.A., Basso, F.G., Hebling, J., de Souza Costa, C.A. (2018). Biological Analysis of Simvastatin-releasing Chitosan Scaffold as a Cell-free System for Pulp-dentin Regeneration. *Journal of Endodontics, 44*(6), 971-976.e1.
13. Lei, Y., Xu, Z., Ke, Q., Yin, W., Chen, Y., Zhang, C., Guo, Y. (2017). Strontium hydroxyapatite/chitosan nanohybrid scaffolds with enhanced osteoinductivity for bonetissue engineering. *Materials Science and Engineering C: Materials for Biological Applications,* 72, 134-142.
14. Kim, H.L., Jung, G.Y., Yoon, J.H., Han, J.S., Park, Y.J., Kim, D.G., Zhang, M., Kim, D.J. (2015). Preparation and characterization of nano-sized hydroxyapatite/alginate/chitosan compositescaffolds for bone tissue engineering. *Materials Science and Engineering C: Materials for Biological Applications*, 54, 20-5.
15. Nitta, S., Komatsu, A., Ishii, T., Ohnishi, M., Inoue, A., Iwamoto, H. (2017). Fabrication and characterization of water-dispersed chitosan nanofiber/poly(ethylene glycol) diacrylate/calcium phosphate-based porous composites. *Carbohydrate Polymer, 174*, 1034-1040.
16. Klein-Júnior, C.A., Reston, E., Plepis, A.M., Martins, V.C., Pötter, I.C., Lundy, F., Hentschke, G.S., Hentschke, V.S., Karim, I.E. (2018). Development and evaluation of calcium hydroxide-coated, pericardium-based biomembranes for direct pulp capping. *Journal of Investigative and Clinical Dentistry*, doi: 10.1111/jicd.12380. [Epub ahead of print]
17. Shahbazarab, Z., Teimouri, A., Chermahini, A.N., Azadi, M. (2018). Fabrication and characterization of nanobiocomposite scaffold of zein/chitosan/nanohydroxyapatite prepared by freeze-drying method for bone tissue engineering. *International Journal of Biological Macromolecules, 108*, 1017-1027.
18. Gupte, M.J., Swanson, W.B., Hu, J., Jin, X., Ma, H., Zhang, Z., Liu, Z., Feng, K., Feng, G., Xiao, G., Hatch, N., Mishina, Y., Ma, P.X. (2018). Pore size directs bone marrow stromal cell fate and tissue regeneration in nanofibrous macroporous scaffolds by mediating vascularization. *Acta Biomaterialia, 82,* 1-11.
19. Madihally, S.V., Matthew, H.W. (1999). Porous chitosan scaffolds for tissue engineering. *Biomaterials, 20*(12), 1133-42.
20. Zhu, Y., Wan, Y., Zhang, J., Yin, D., Cheng, W. (2014). Manufacture of layered collagen/chitosan-polycaprolactone scaffolds with biomimeticmicroarchitecture. *Colloids Surface B Biointerfaces, 113*, 352-60.
21. Aranaz, I., Martínez-Campos, E., Moreno-Vicente, C., Civantos, A., García-Arguelles, S., Del Monte, F. (2017). Macroporous Calcium Phosphate/Chitosan Composites Prepared via Unidirectional Ice Segregation and Subsequent Freeze-Drying. *Materials (Basel), 10*(5), 516; doi:10.3390/ma10050516

22. Ruixin, L., Dong, L., Bin, Z., Hao, L., Xue, L., Caihong, S., Weihua, S., Xiaoli, Q., Yinghai, Y., Weining, A., Xizheng, Z. (2016). A mechanical evaluation of micro-HA/CS composite scaffolds with interconnected spherical macropores. *Biomedical Engineering Online, 15*, 12.
23. Ruixin, L., Cheng, X., Yingjie, L., Hao, L., Caihong, S., Weihua, S., Weining, A., Yinghai, Y., Xiaoli, Q., Yunqiang, X., Xizheng, Z., Hui, L. (2017). Degradation behavior and compatibility of micro, nanoHA/chitosan scaffolds with interconnectedspherical macropores. *International Journal of Biological Macromolecules, 103*, 385-394.
24. Wang, D., Liu , Feng, Q2., Dong, C., Liu, Q., Duan, L., Huang, J., Zhu, W., Li, Z., Xiong, J., Liang, Y., Chen, J., Sun, R5., Bian, L., Wang, D. (2017). Effect of inorganic/organic ratio and chemical coupling on the performance of poroussilica/chitosan hybrid scaffolds. *Materials Science and Engineering C: Materials for Biological Applications, 70*(Pt 2), 969-975.
25. Wang, Y., Qian, J., Zhao, N., Liu, T., Xu, W., Suo, A. (2017). Novel hydroxyethyl chitosan/cellulose scaffolds with bubble-like porous structure for bone tissue engineering. *Carbohydrate Polymers, 167*, 44-51.
26. Harris, L.D., Kim, B.S., Mooney, D.J. (1998). Open pore biodegradable matrices formed with gas foaming. Journal of Biomedical. *Materials Research, 42*(3), 396-402.
27. Kim, C.W., Talac, R., Lu, L., Moore, M.J., Currier, B.L., Yaszemski, M.J. (2008). Characterization of porous injectable poly-(propylene fumarate)-based bone graft substitute. *Journal of Biomedical Materials Research A, 85*(4), 1114-9.
28. Chen, W., Zhou, H., Tang, M., Weir, M.D., Bao, C., Xu, H.H. (2012). Gas-foaming calcium phosphate cement scaffold encapsulating human umbilical cord stem cells. *Tissue Engineering Part A, 18*(7-8), 816-27.
29. Thein-Han, W., Xu, H.H. (2013). Prevascularization of a gas-foaming macroporous calcium phosphate cement scaffold viacoculture of human umbilical vein endothelial cells and osteoblasts. *Tissue Engineering Part A, 19(*15-16), 1675-85.
30. Chen, W., Thein-Han, W., Weir, M.D., Chen, Q., Xu, H.H. (2014). Prevascularization of biofunctional calcium phosphate cement for dental and craniofacial repairs. *Dental Materials, 30*(5), 535-44.
31. Sergeeva, A.S., Gorin, D.A., Volodkin, D.V. (2015). In-situ assembly of Ca-alginate gels with controlled pore loading/release capability. *Langmuir, 31*(39), 10813-21.
32. Holopainen, J., Santala, E., Heikkilä, M., Ritala, M. (2014). Electrospinning of calcium carbonate fibers and their conversion to nanocrystallinehydroxyapatite. *Materials Science and Engineering C: Materials for Biological Applications, 45*, 469-76.
33. Wang, L., Zhang, C., Li, C., Weir, M.D., Wang, P., Reynolds, M.A., Zhao, L., Xu, H.H. (2016). Injectable calcium phosphate with hydrogel fibers encapsulating induced pluripotent, dental pulp and bone marrow stem cells for bone repair. *Materials Science and Engineering C: Materials for Biological Applications, 69*, 1125-36.

34. Diaz-Rodriguez, P., Garcia-Triñanes, P., Echezarreta López, M.M., Santoveña, A., Landin, M. (2018). Mineralized alginate hydrogels using marine carbonates for bone tissue engineering applications. *Carbohydrate Polymers, 195*, 235-242.
35. Saveleva, M.S., Ivanov, A.N., Kurtukova, M.O., Atkin, V.S., Ivanova, A.G., Lyubun, G.P., Martyukova, A.V., Cherevko, E.I., Sargsyan. A.K., Fedonnikov, A.S., Norkin, I.A., Skirtach, A.G., Gorin, D.A., Parakhonskiy, B.V. (2018). Hybrid PCL/CaCO3 scaffolds with capabilities of carrying biologically active molecules: Synthesis, loading and in vivo applications. *Materials Science and Engineering C: Materials for Biological Applications, 85*, 57-67.
36. Mohan, N., Palangadan, R., Fernandez, F.B., Varma, H. (2018). Preparation of hydroxyapatite porous scaffold from a 'coral-like' synthetic inorganic precursor for use as a bone substitute and a drug delivery vehicle. *Materials Science and Engineering C: Materials for Biological Applications, 92*, 329-337.
37. Savija Rashid, F., Shiba, H., Mizuno, N., Mouri, Y., Fujita, T., Shinohara, H., Ogawa, T., Kawaguchi, H., Kurihara, H. (2003). The effect of extracellular calcium ion on gene expression of bone-related proteins in human pulp cells. *Journal of Endodontics, 29*(2), 104-7.
38. Plavsic, B., Kobe, S., Orel, B. (1999). Identification of crystallization forms of CaCO3 with FTIR. Spectroscopy KZLTET, 33(6), 517.
39. Kim, M.J., Kim, D. (2018). Maximization of CO2 storage for various solvent types in indirect carbonation using paper sludgeash. *Environmental Science and Pollution Research, 25*(30), 30101-30109.
40. Vinoba, M., Bhagiyalakshmi, M., Grace, A.N., Chu, D.H., Nam, S.C., Yoon, Y., Yoon, S.H., Jeong, S.K. (2013). CO2 absorption and sequestration as various polymorphs of CaCO3 using sterically hinderedamine. *Langmuir, 29*(50), 15655-63.
41. Kim, H.L., Jung, G.Y., Yoon, J.H., Han, J.S., Park, Y.J., Kim, D.G., Zhang, M., Kim, D.J. (2015). Preparation and characterization of nano-sized hydroxyapatite/alginate/chitosan compositescaffolds for bone tissue engineering. *Materials Science and Engineering C: Materials for Biological Applications*, 54, 20-5.
42. He, Q., Ao, Q., Gong, Y., Zhang, X. (2011). Preparation of chitosan films using different neutralizing solutions to improve endothelial cellcompatibility. *Journal of Materials Science: Materials in Medicine, 22*(12), 2791-802.
43. Pestov, A., Bratskaya, S. (2016). Chitosan and Its Derivatives as Highly Efficient Polymer Ligands. *Molecules, 21*(3), 330.
44. Volda, I.M.N., Varuma, K.M., Guibalb, E., Smidsrøda, O. (2003). Binding of ions to chitosan—selectivity studies. *Carbohydrate Polymers, 54*, 471–477.
45. Chen, Z.G., Wang, P.W., Wei, B., Mo, X.M., Cui, F.Z. (2010). Electrospun collagen-chitosan nanofiber: a biomimetic extracellular matrix for endothelial cell and smooth muscle cell. *Acta Biomaterialia, 6*(2), 372-82.

46. Liu, Y., Wang, S., Zhang, R. (2017). Composite poly(lactic acid)/chitosan nanofibrous scaffolds for cardiac tissue engineering. *International Journal of Biological Macromolecules*, 103, 1130-1137.
47. Zhu, B., Li, W., Chi, N., Lewis, R.V., Osamor, J., Wang, R. (2017). Optimization of Glutaraldehyde Vapor Treatment for Electrospun Collagen/Silk Tissue Engineering Scaffolds. *ACS Omega, 2*(6), 2439-2450.
48. Kim, H.L., Jung, G.Y., Yoon, J.H., Han, J.S., Park, Y.J., Kim, D.G., Zhang, M., Kim, D.J. (2015). Preparation and characterization of nano-sized hydroxyapatite/alginate/chitosan compositescaffolds for bone tissue engineering. *Materials Science and Engineering C: Materials for Biological Applications*, 54, 20-5.
49. Farhadian, N., Godiny, M., Moradi, S., Hemati Azandaryani, A., Shahlaei, M. (2018). Chitosan/gelatin as a new nano-carrier system for calcium hydroxide delivery in endodonticapplications: Development, characterization and process optimization. *Materials Science and Engineering C: Materials for Biological Applications*, *92*, 540-546.
50. Klein-Júnior, C.A., Reston, E., Plepis, A.M., Martins, V.C., Pötter, I.C., Lundy, F., Hentschke, G.S., Hentschke, V.S., Karim, I.E. (2018). Development and evaluation of calcium hydroxide-coated, pericardium-based biomembranes for direct pulp capping. *Journal of Investigative and Clinical Dentistry*, doi: 10.1111/jicd.12380. [Epub ahead of print]
51. Rashid, F., Shiba, H., Mizuno, N., Mouri, Y., Fujita, T., Shinohara, H., Ogawa, T., Kawaguchi, H., Kurihara, H. (2003). The effect of extracellular calcium ion on gene expression of bone-related proteins in human pulp cells. *Journal of Endodontics, 29*(2), 104-7.
52. An, S., Gao, Y., Ling, J., Wei, X., Xiao, Y. (2012). Calcium ions promote osteogenic differentiation and mineralization of human dental pulp cells: implications for pulp capping materials. *Journal of Materials Science: Materials in Medicine, 23*(3), 789-95.
53. Barradas, A.M., Fernandes, H.A., Groen, N., Chai, Y.C., Schrooten, J., van de Peppel, J., van Leeuwen, J.P., van Blitterswijk, C.A., de Boer, J. (2012). A calcium-induced signaling cascade leading to osteogenic differentiation of human bone marrow-derived mesenchymal stromal cells. *Biomaterials, 33*(11), 3205-15.
54. Woo, S.M., Hwang, Y.C., Lim, H.S., Choi, N.K., Kim, S.H., Kim, W.J., Kim, S.M., Jung, J.Y. (2013). Effect of nifedipine on the differentiation of human dental pulp cells cultured with mineral trioxide aggregate. *Journal of Endodontics, 39*(6), 801-5.
55. Li, S., Hu, J., Zhang, G., Qi, W., Zhang, P., Li, P., Zeng, Y., Zhao, W., Tan, Y. (2015). Extracellular Ca2+ Promotes Odontoblastic Differentiation of Dental Pulp Stem Cells via BMP2-Mediated Smad1/5/8 and Erk1/2 Pathways. *Journal* of *Cellular Physiology*, 230(9), 2164-73.
56. Kanaya, S., Xiao, B., Sakisaka, Y., Suto, M., Maruyama, K., Saito, M., Nemoto, E. (2018). Extracellular calcium increases fibroblast growth factor 2 gene expression via

extracellular signal-regulated kinase 1/2 and protein kinase A signaling in mouse dental papilla cells. *Journal of Applied Oral Science, 26*, e20170231.

57. Kulan, P., Karabiyik, O., Kose, G.T., Kargul, B. (2018). The effect of accelerated mineral trioxide aggregate on odontoblastic differentiation in dental pulp stem cell niches. *International Endodontic Journal, 51*(7), 758-766.

FIGURE CAPTIONS

Figure 1. Panel of images for selection of the scaffold's composition selection. From left to right, SEM of the scaffold surface (500 x), EDS graphs, and Live/Dead assay 24 h after HDPC seeding (20 x), representative of the scaffolds formulated with: (a) 1% high molecular weight chitosan solution, (b) 1% high molecular weight chitosan solution + 1% Ca(OH2) suspension 2:1, (c) 2% high molecular weight chitosan solution, (d) 1% high molecular weight chitosan solution + 1% Ca(OH2) suspension 2:1. Green fluorescence indicates live cells. Red fluorescence indicates dead cells. Full white arrows indicate cells organized in clusters; the open white arrow indicates cells exhibiting wide cytoplasm spreading throughout the scaffold.

Figure 2. Panel of SEM (200 x) images (a) Bar graphs of pore diameter, (b) overall porosity, and (c) of CH-Ca scaffolds subjected to the different freezing protocols. Bars are mean (numbers) and standard-deviation of the pore diameter (μm) and overall porosity (%). [indicates significant differences among the groups (one-way ANOVA; Tukey's test; $p<0.05$. n=6).

Figure 3. FTIR spectrum comparing (a) CH and CH-Ca scaffold before cross-linking; (b) CH before and after cross-linking; (c) CH-Ca before and after cross-linking; and (d) CH and CH-Ca scaffold after cross-linking

Figure 4. Characterization of cross-linked scaffolds. (a) and (b) Representative SEM images at low and high magnification of the surface (left) and transversal slice (right) of CH; (c) and (d) – Representative SEM images at low and high magnification of surface (left) and transversal slice (right) of CH-Ca. The white arrows indicate pore interconnectivity; (e) and (f) Bar graphs of pore diameter and overall porosity, respectively. Bars are the mean (numbers) and standard-deviation of the pore diameter (μm) and overall porosity (%). [indicates significant differences among groups (Student's t-test; $p<0.05$. n=6)

Figure 5. Calcium release assay from CH and CH-Ca cross-linked scaffolds incubated in ultra-pure distillated water at 37°C, for 21 days (n=4). Values are mean and standard deviation of cumulative calcium released (mg/dL in ultra-pure water), at 1, 5, 7, 14, and 21 days.

Figure 6. Cytocompatibility assay for cross-linked scaffolds. (a) Alamar blue. Bar graph of the mean values for cell viability percentage at each timepoint for both scaffolds. Letters allow comparisons among the timepoints, for each scaffold. [Allows comparisons among scaffolds at each timepoint (Two-way ANOVA; Tukey's test; $p < 0.05$. n=6). (b) Representative images of Live/Dead assay at the scaffold surface. Green = live cells; Red = dead cells. (c) and (d) – Representative images of F-actin staining at

the material's surface and transversal slices, respectively. Red = actin filaments; Blue = nuclei.]

Figure 7. Bioactivity assays for cross-linked scaffolds. (a) ALP activity (% of ug/mg protein from CH group), (b-e) gene expression of ALP, Col1, DMP-1 and DSPP ($2^{\Delta\Delta CT}$), respectively; and (f) Alizarin red assay (% alizarin red staining from CH group). Bar graphs of mean values for each cell parameter for both scaffolds. [Allows comparisons among scaffolds, at each timepoint (Student's t-test; $p < 0.05$. $n = 6$)].

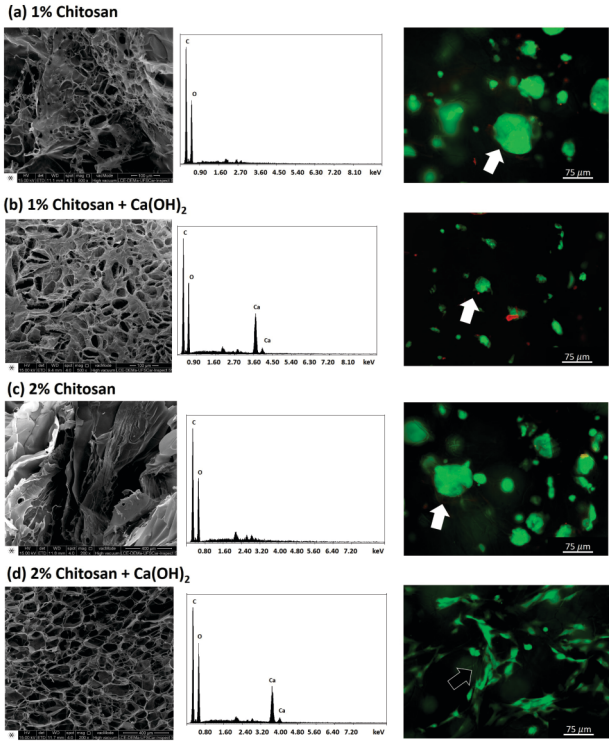

JBMB_34586_fig1.tif

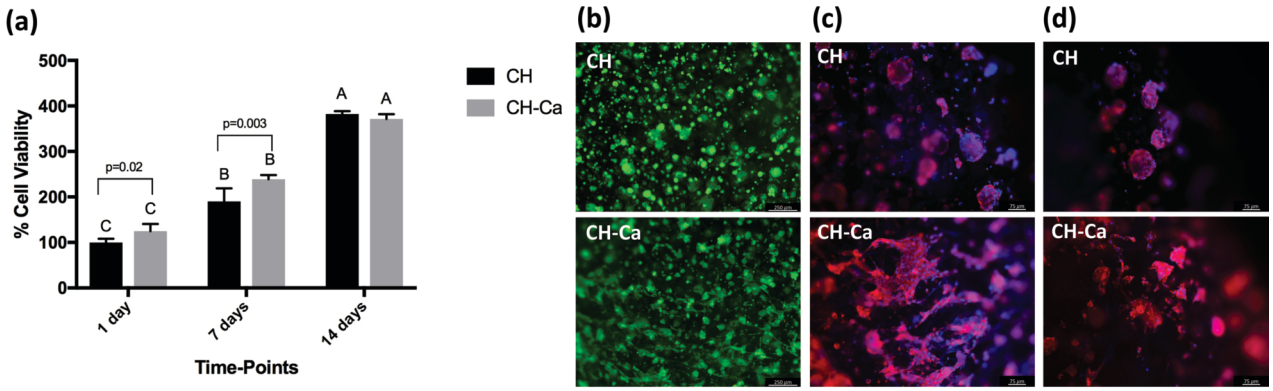

JBMB_34586_fig6.tif

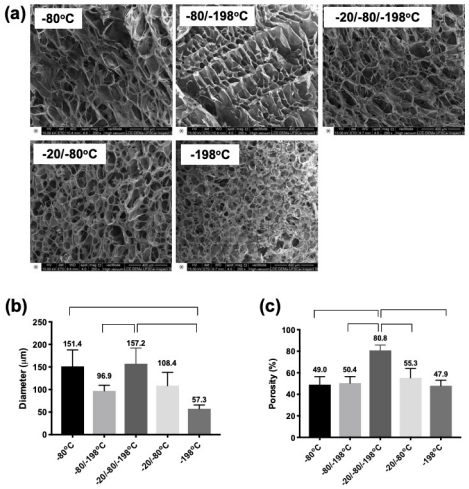

JBMB_34586_Fig2.tiff

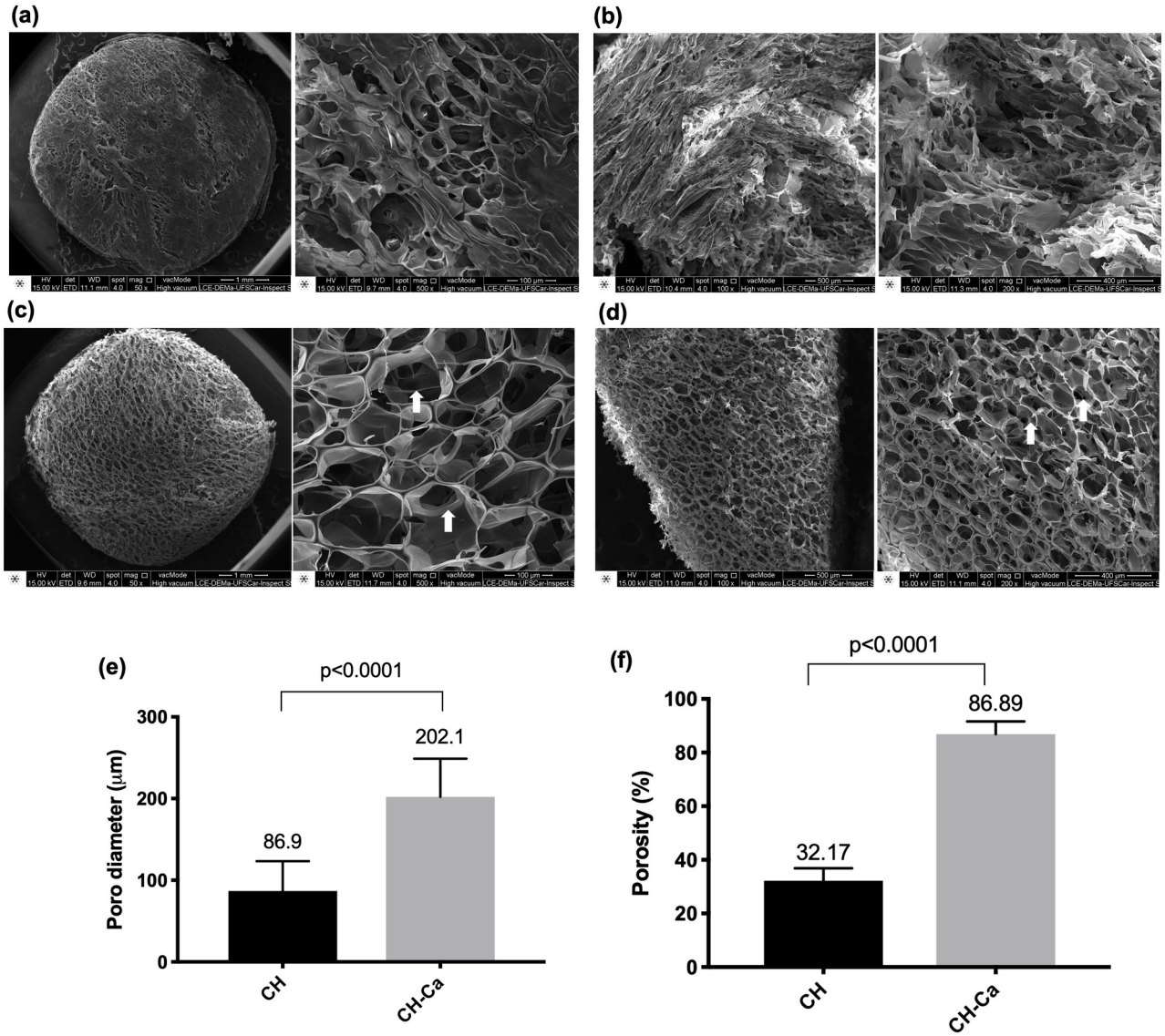

JBMB_34586_Fig4.tiff

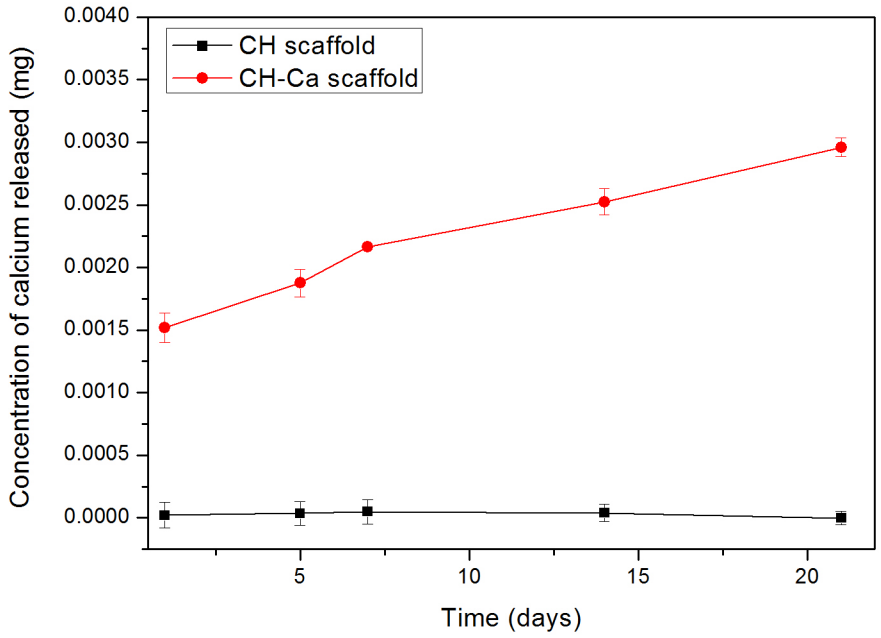

JBMB_34586_Fig5.tiff

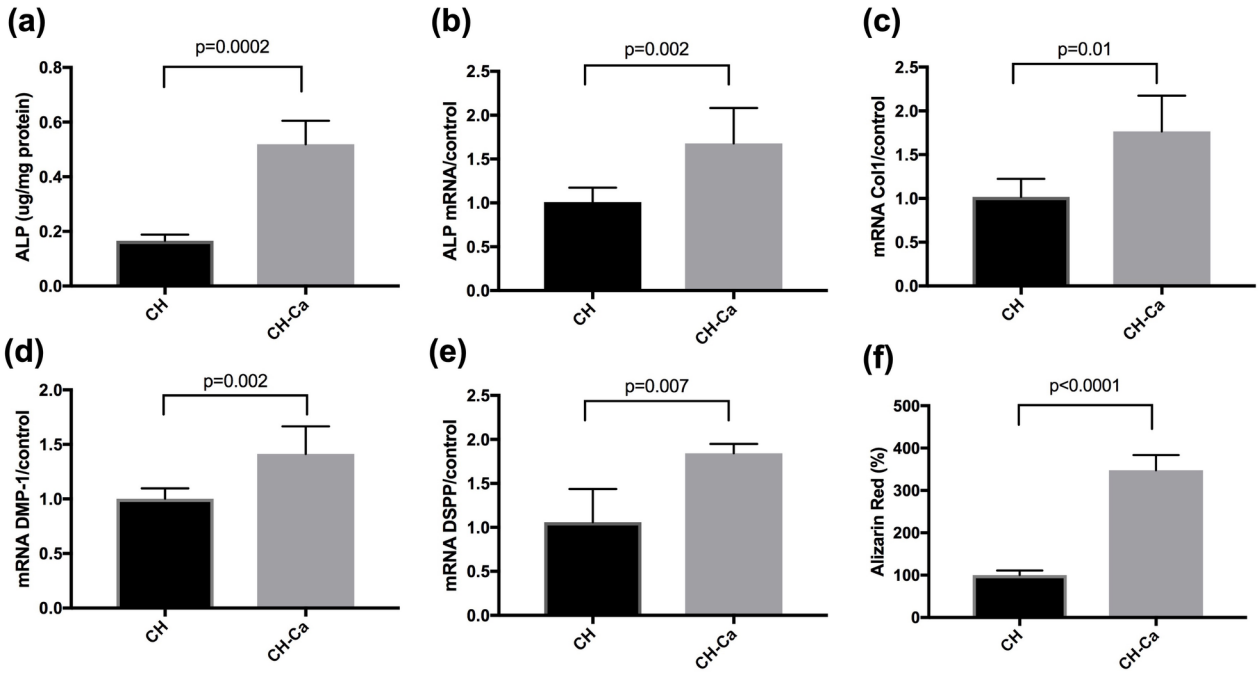

JBMB_34586_Fig7.tiff

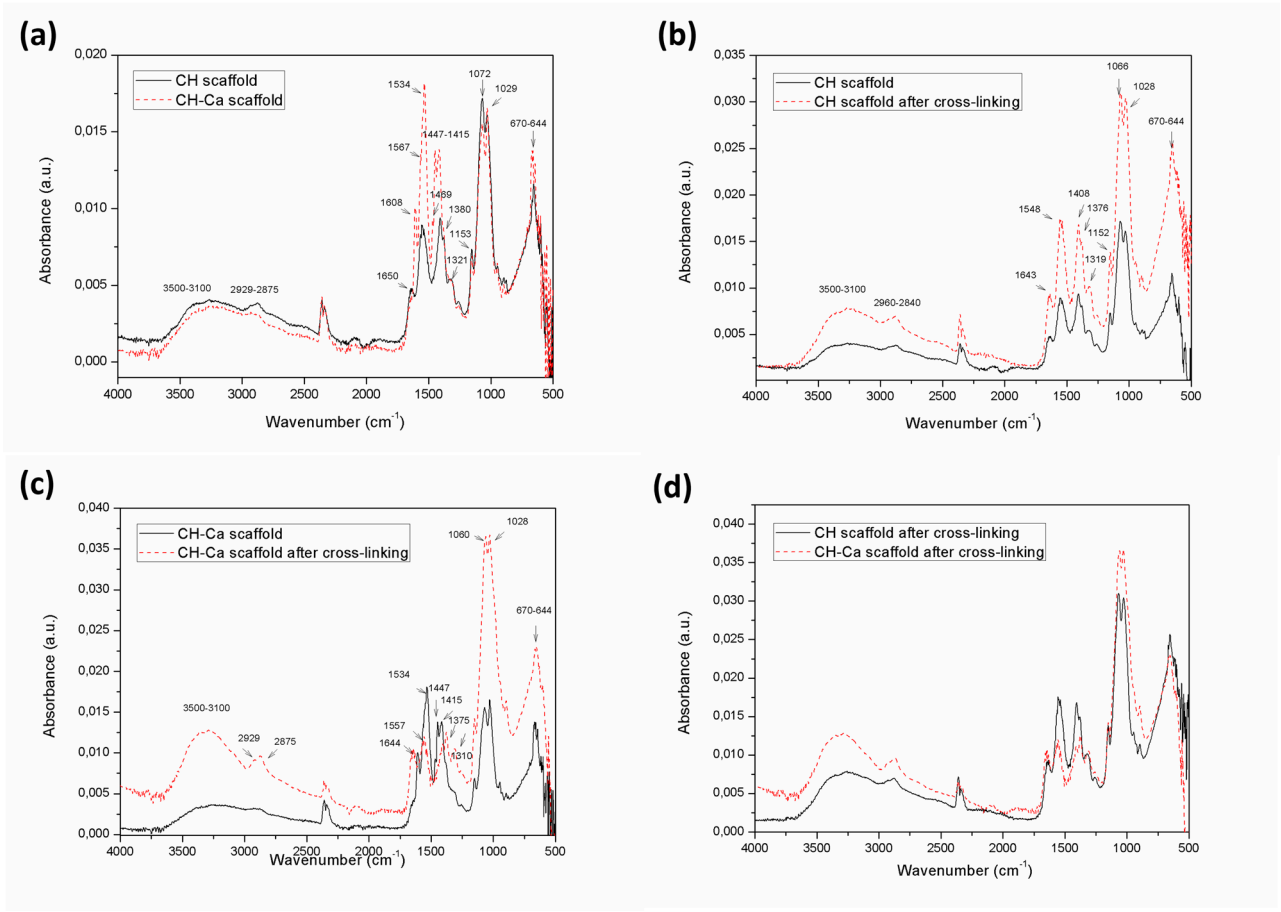

JBMB_34586_Fig 3 (revised) final.tif

Table 1. Effect of cross-linking with GA vapor on scaffold degradation.

GROUPS							
Scaffold	**Cross-linking**	**Baseline**	**1 day**	**7 days**	**14 days**	**21 days**	**28 days**
CH	-	100.00* (± 15.89)** Aa	104.79 (± 19.58) Aa	68.30 (± 14.81) Bb	25.75 (± 7.46) Cb	16.09 (± 4.97) Cb	14.06 (± 4.71) Cc
CH	+	100.00 (± 9.42) Aa	98.00 (± 8.40) Aa	109.81 (± 14.78) Aa	111.63 (± 30.39) Aa	94.08 (± 10.28) Aa	92.90 (± 5.29) Aa
CH-Ca	-	100.00 (± 19.94) Aa	71.11 (± 14.04) Bb	45.01 (± 1.16) Cb	15.66 (± 1.92) Db	8.57 (± 0.87) Db	5.83 (± 0.95) Dc
CH-Ca	+	100.00 (± 12.04) Aa	94.85 (± 14.94) ABab	106.71 (± 20.54) ABa	90.48 (± 26.65) ABa	73.96 (± 11.42) BCa	57.81 (± 10.58) Cb

*Mean values of humid weight percentage. ** standard deviation. Upper-case letters allow comparisons in lines and lower-case letters allow comparisons in rows ($p < 0,05$; repeated measure two-way ANOVA, Tukey's test; $n = 6$).